Progress In Electromagnetics Research, PIER 72, 91–103, 2007

ENHANCEMENT OF TM-TE MODE CONVERSION CAUSED BY EXCITATION OF SURFACE PLASMONS ON A METAL GRATING AND ITS APPLICATION FOR REFRACTIVE INDEX MEASUREMENT

T. Suyama and Y. Okuno

Graduate School of Science and Technology
Kumamoto University
2-39-1 Kurokami, Kumamoto 860-8555, Japan

T. Matsuda

Kumamoto National College of Technology
2659-2 Suya, Nishigoshi 861-1102, Japan

Abstract—Yasuura's mode-matching method is employed in the investigation of plasmon resonance absorption on a metal grating with a gold over-coating and the results are compared with experimental data. Enhancement of TM-TE mode conversion accompanying the plasmon resonance absorption is examined. When a TM wave is incident on a metal grating, enhanced TM-TE mode conversion occurs at angles of incidence at which the surface plasmons are excited. The strength of the mode conversion depends strongly on the azimuth angle of the mounting. This is verified by experiment and an application for refractive index measurement is suggested.

1. INTRODUCTION

A metal grating has an interesting property known as the resonance absorption in the optics region [1]: partial or total absorption of incident light occurs at a specific angle of incidence, which is called a resonance angle. This is caused by excitation of plasmon surface waves and is accompanied by an abrupt change of diffraction efficiency known as a resonance anomaly [1–3]. For a grating placed in planar (or classical) mounting (the plane of incidence is perpendicular to the grooves) this phenomenon can be seen in TM incidence alone. While in conical mounting (the plane of incidence is not perpendicular

to the grooves) the absorption is observed in both TM and TE incidence; and the absorption is accompanied by enhanced TM-TE mode conversion [4, 5]. Although the mode conversion always occurs in conical mounting, it is enhanced by the excitation of surface plasmons. In fact, when the resonance absorption occurs, the TM-component of the reflected wave almost vanishes and the TE-component is dominant. The TM-TE mode conversion can be a practical measure in finding the resonance angle.

Although a plasmon index sensor with a prism has been examined by many researchers in detail, few works with a metal grating can be seen. We examine the possibility of employing the plasmon resonance absorption as an index sensor comparing the numerical results with experimental data. We show that the use of polarization conversion accompanying the resonance absorption is necessary in designing a precise measurement system.

2. FORMULATION AND THE METHOD OF SOLUTION

This section deals with the theoretical part of the present work: statement of the problem and a concise introduction of the method of solution. In this paper, a time factor $\exp(-i\omega t)$ is suppressed.

2.1. Statement of the Problem

Figure 1 shows the schematic representation of diffraction by a layered grating made of a metal and having an over-coating made of another metal. The grating is uniform in the Y direction and is periodic in X. The surface profiles are given by

$$\begin{aligned} \mathrm{S}_1 : z_1 &= \eta_1(x) = h\sin(2\pi x/d) \\ \mathrm{S}_2 : z_2 &= \eta_2(x) = \eta_1(x) - e \end{aligned} \tag{1}$$

where h, d, and e are the amplitude (half depth) of the surface modulation, the period, and the thickness of the coating. Note that the small letters (x, y, z) denote a point on the surface. The surfaces separate the whole space into three regions:

$$\begin{aligned} &\mathrm{V}_1 : Z > \eta_1(X) \text{ (free space)} \\ &\mathrm{V}_2 : \eta_1(X) < Z < \eta_2(X) \text{ (metal-coating)} \\ &\mathrm{V}_3 : Z < \eta_2(X) \text{ (metal)} \end{aligned} \tag{2}$$

We assume that V_1, V_2 and V_3, respectively, are filled with a dielectric (with a positive refractive index n_1), a metal (having a

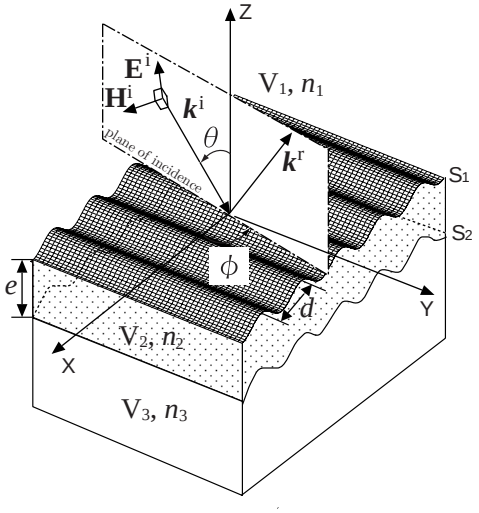

Figure 1. Schematic representation of diffraction by a metal grating with gold over-coating.

complex-valued index n_2), and another metal (with a complex n_3). Note that the capital letters (X, Y, Z) show the coordinates of a point in these regions. A convention $\boldsymbol{P} = (X, Y, Z)$ will be used as well. The electric and magnetic field of an incident light is given by

$$\begin{pmatrix} \boldsymbol{E}^{\mathrm{i}} \\ \boldsymbol{H}^{\mathrm{i}} \end{pmatrix} (\boldsymbol{P}) = \begin{pmatrix} \boldsymbol{e}^{\mathrm{i}} \\ \boldsymbol{h}^{\mathrm{i}} \end{pmatrix} \exp(i\boldsymbol{k}^{\mathrm{i}} \cdot \boldsymbol{P}) \tag{3}$$

with

$$\boldsymbol{h}^{\mathrm{i}} = (1/\omega\mu_0)\, \boldsymbol{k}^{\mathrm{i}} \times \boldsymbol{e}^{\mathrm{i}} \tag{4}$$

Here, $\boldsymbol{e}^{\mathrm{i}}$ is the electric-field amplitude and $\boldsymbol{k}^{\mathrm{i}}$ is the incident wave vector

$$\boldsymbol{k}^{\mathrm{i}} = (\alpha,\ \beta,\ -\gamma) \tag{5}$$

with $\alpha = n_1 k^{\mathrm{i}} \sin\theta\cos\phi$, $\beta = n_1 k^{\mathrm{i}} \sin\theta\sin\phi$, $\gamma = n_1 k^{\mathrm{i}} \cos\theta$, and $k^{\mathrm{i}} = 2\pi/\lambda$. As shown in Fig. 1, θ is a polar angle between the Z-axis and the incident wave vector and ϕ is an azimuth angle between the X-axis and the plane of incidence. When $\phi = 0°$, the incident light comes from a direction orthogonal to the grooves and the diffracted waves propagate in directions in the plane of incidence. This arrangement is called *planar* (or classical) *mounting*. While if $\phi \neq 0°$, as shown in Fig. 1, the directions lie on a cone centered at the origin. This is termed *conical mounting*.

Let us decompose the amplitude of the incident light into a TE- and a TM-component, where TE (or TM) means the absence of the Z-component in the relevant electric (or magnetic) field. To do this, we first define two unit vectors that span a plane orthogonal to $\boldsymbol{k}^{\mathrm{i}}$:

$$\boldsymbol{e}^{\mathrm{TE}} = (\sin\phi, -\cos\phi, 0) \tag{6}$$

$$\boldsymbol{e}^{\mathrm{TM}} = (\cos\theta\cos\phi, \cos\theta\sin\phi, \sin\theta) \tag{7}$$

Apparently, $\boldsymbol{e}^{\mathrm{TE}}$ has no Z-component. The fact that the magnetic amplitude accompanying $\boldsymbol{e}^{\mathrm{TM}}$ cannot have any Z-component is seen by direct manipulation. In addition, they are perpendicular to each other, and both of them make a right angle with $\boldsymbol{k}^{\mathrm{i}}$. Hence, they are the unit vectors in the direction of the TE- and TM-component in the sense above. The amplitude $\boldsymbol{e}^{\mathrm{i}}$ is decomposed as

$$\boldsymbol{e}^{\mathrm{i}} = \cos\delta\boldsymbol{e}^{\mathrm{TE}} + \sin\delta\boldsymbol{e}^{\mathrm{TM}} \tag{8}$$

where δ is the angle between $\boldsymbol{e}^{\mathrm{TE}}$ and $\boldsymbol{e}^{\mathrm{i}}$ (see Fig. 2) and is termed a polarization angle. In particular, $\delta = 0^\circ$ means TE incidence and $\delta = 90^\circ$ stands for TM incidence. Thus the incident light is specified by the wavelength λ, the polar angle θ, the azimuth angle ϕ, and the polarization angle δ. In this paper, we only consider the case of TM incidence ($\delta = 90^\circ$).

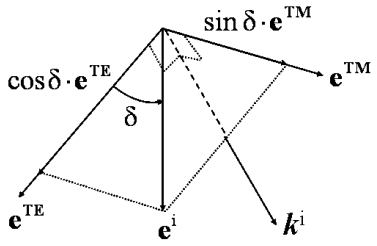

Figure 2. Definition of the polarision angle.

We consider the problem to seek the diffracted electric and magnetic fields in V_j ($j = 1, 2, 3$). Note that they consist of both TE- and TM-components. The solutions should satisfy the following requirements:

D1: The Helmholtz equations in each region;

D2: A radiation condition in the Z-direction that the diffracted waves in V_1 (or V_3) propagate or attenuate in positive (or negative) Z direction;

D3: A periodicity condition that: for any component of diffracted light, the relation $f(X+d,Y,Z) = e^{i\alpha d} f(X,Y,Z)$ holds and the phase constant in Y is β; and

D4: The boundary conditions on S_1 and S_2 that the tangential components of the electric and magnetic fields must be continuous across the boundary.

2.2. Method of Solution

Because the diffracted fields have both TE- and TM-components, we need TE and TM vector modal functions to construct the solutions. The modal functions are derived from the Floquet modes (separated solutions of the Helmholtz equation satisfying the radiation and the periodicity condition) and are defined by

$$\begin{aligned} \boldsymbol{\varphi}_{jm}^{\mathrm{TE}}(\boldsymbol{P}) &= \boldsymbol{e}_{jm}^{\mathrm{TE}} \exp(i\boldsymbol{k}_{jm} \cdot \boldsymbol{P}) \\ \boldsymbol{\varphi}_{jm}^{\mathrm{TM}}(\boldsymbol{P}) &= \boldsymbol{e}_{jm}^{\mathrm{TM}} \exp(i\boldsymbol{k}_{jm} \cdot \boldsymbol{P}) \\ m &= 0, \pm 1, \pm 2, \ldots (\boldsymbol{P} \in \mathrm{V}_j;\ j = 1,2,3) \end{aligned} \tag{9}$$

with

$$\begin{aligned} \boldsymbol{e}_{jm}^{\mathrm{TE}} &= \boldsymbol{k}_{jm} \times \boldsymbol{i}_Z / |\boldsymbol{k}_{jm} \times \boldsymbol{i}_Z| \\ \boldsymbol{e}_{jm}^{\mathrm{TM}} &= \boldsymbol{e}_{jm}^{\mathrm{TE}} \times \boldsymbol{k}_{jm} \Big/ \left|\boldsymbol{e}_{jm}^{\mathrm{TE}} \times \boldsymbol{k}_{jm}\right| \end{aligned} \tag{10}$$

Here, $\boldsymbol{i}_Z$ is a unit vector in the Z-direction and

$$\begin{aligned} \boldsymbol{k}_{1m} &= (\alpha_m, \beta, \gamma_{1m}) \\ \boldsymbol{k}_{2m} &= (\alpha_m, \beta, \mp\gamma_{2m}) \\ \boldsymbol{k}_{3m} &= (\alpha_m, \beta, -\gamma_{3m}) \end{aligned} \tag{11}$$

are the wave vectors of the mth order diffracted modes in V_j with

$$\alpha_m = \alpha + 2m\pi/d \tag{12}$$

and

$$\gamma_{jm}^2 = (n_j k)^2 - (\alpha_m^2 + \beta^2),\ \mathrm{Im}(\gamma_{jm}) \geq 0 \tag{13}$$

Note that the modal functions given in (9) are used in constructing the diffracted electric fields. For the magnetic fields another set of modal function can be obtained from (9) though Maxwell's equations as:

$$\boldsymbol{\psi}_{jm}^{q}(\boldsymbol{P}) = (1/\omega\mu_0)\boldsymbol{k}_{jm} \times \boldsymbol{\varphi}_{jm}^{q}(q = \mathrm{TE},\ \mathrm{TM}) \tag{14}$$

Approximate solutions in V_1 are defined as finite linear combinations of up-going modal functions with unknown modal

coefficients. Likewise, the solutions in V_3 are finite sums of down-going modal functions. Whereas the solutions in V_2 must have both up- and down-going modal functions. All the solutions, of course, should consist of TE- and TM-components unless the planar mounting case. The approximate solutions in each region, hence, can be expressed as:

$$\begin{aligned}
\begin{pmatrix} \boldsymbol{E}^{\mathrm{d}}_{1N} \\ \boldsymbol{H}^{\mathrm{d}}_{1N} \end{pmatrix}(\boldsymbol{P}) &= \sum_{n=-N}^{N} A^{\mathrm{TE}}_{1n}(N) \begin{pmatrix} \boldsymbol{\varphi}^{\mathrm{TE}}_{1n} \\ \boldsymbol{\psi}^{\mathrm{TE}}_{1n} \end{pmatrix}(\boldsymbol{P}) \\
&\quad + \sum_{n=-N}^{N} A^{\mathrm{TM}}_{1n}(N) \begin{pmatrix} \boldsymbol{\varphi}^{\mathrm{TM}}_{1n} \\ \boldsymbol{\psi}^{\mathrm{TM}}_{1n} \end{pmatrix}(\boldsymbol{P}) \\
\begin{pmatrix} \boldsymbol{E}^{\mathrm{d}}_{2N} \\ \boldsymbol{H}^{\mathrm{d}}_{2N} \end{pmatrix}(\boldsymbol{P}) &= \sum_{n=-N}^{N} A^{\mathrm{TE}-}_{2n}(N) \begin{pmatrix} \boldsymbol{\varphi}^{\mathrm{TE}-}_{2n} \\ \boldsymbol{\psi}^{\mathrm{TE}-}_{2n} \end{pmatrix}(\boldsymbol{P}) \\
&\quad + \sum_{n=-N}^{N} A^{\mathrm{TM}-}_{2n}(N) \begin{pmatrix} \boldsymbol{\varphi}^{\mathrm{TM}-}_{2n} \\ \boldsymbol{\psi}^{\mathrm{TM}-}_{2n} \end{pmatrix}(\boldsymbol{P}) \\
&\quad + \sum_{n=-N}^{N} A^{\mathrm{TE}+}_{2n}(N) \begin{pmatrix} \boldsymbol{\varphi}^{\mathrm{TE}+}_{2n} \\ \boldsymbol{\psi}^{\mathrm{TE}+}_{2n} \end{pmatrix}(\boldsymbol{P}) \\
&\quad + \sum_{n=-N}^{N} A^{\mathrm{TM}+}_{2n}(N) \begin{pmatrix} \boldsymbol{\varphi}^{\mathrm{TM}+}_{2n} \\ \boldsymbol{\psi}^{\mathrm{TM}+}_{2n} \end{pmatrix}(\boldsymbol{P}) \qquad (15) \\
\begin{pmatrix} \boldsymbol{E}^{\mathrm{d}}_{3N} \\ \boldsymbol{H}^{\mathrm{d}}_{3N} \end{pmatrix}(\boldsymbol{P}) &= \sum_{n=-N}^{N} A^{\mathrm{TE}}_{3n}(N) \begin{pmatrix} \boldsymbol{\varphi}^{\mathrm{TE}}_{3n} \\ \boldsymbol{\psi}^{\mathrm{TE}}_{3n} \end{pmatrix}(\boldsymbol{P}) \\
&\quad + \sum_{n=-N}^{N} A^{\mathrm{TM}}_{3n}(N) \begin{pmatrix} \boldsymbol{\varphi}^{\mathrm{TM}}_{3n} \\ \boldsymbol{\psi}^{\mathrm{TM}}_{3n} \end{pmatrix}(\boldsymbol{P}) \qquad (16)
\end{aligned}$$

where N is the number of truncation and the plus and minus sign represent the direction of propagation. Thus an approximate representation of the total electric (or magnetic) field in V_1 is a sum of $\boldsymbol{E}^{\mathrm{i}}(\boldsymbol{P})$ and $\boldsymbol{E}^{\mathrm{d}}_{1N}(\boldsymbol{P})$ (or $\boldsymbol{H}^{\mathrm{i}}(\boldsymbol{P})$ and $\boldsymbol{H}^{\mathrm{d}}_{1N}(\boldsymbol{P})$). While $\boldsymbol{E}^{\mathrm{d}}_{2N}(\boldsymbol{P})$ and $\boldsymbol{H}^{\mathrm{d}}_{2N}(\boldsymbol{P})$ (or $\boldsymbol{E}^{\mathrm{d}}_{3N}(\boldsymbol{P})$ and $\boldsymbol{H}^{\mathrm{d}}_{3N}(\boldsymbol{P})$) are the representations in V_2 (or V_3).

Since the approximate solutions already satisfy the requirements (D1), (D2), and (D3), the modal coefficients should be determined in order that the solutions satisfy the boundary condition (D4) in an approximate sense. According to Yasuura's theory [6–8], we determine the coefficients by the least-squares method. That is, we find the

coefficients that minimize the quadratic form

$$\begin{aligned} I_N \;=\; & \int_{\mathrm{S}_1} \left| \boldsymbol{\nu} \times [\boldsymbol{E}^{\mathrm{d}}_{1N} + \boldsymbol{E}^{\mathrm{i}} - \boldsymbol{E}^{\mathrm{d}}_{2N}](s) \right|^2 ds \\ & + \int_{\mathrm{S}_2} \left| \boldsymbol{\nu} \times [\boldsymbol{E}^{\mathrm{d}}_{2N} - \boldsymbol{E}^{\mathrm{d}}_{3N}](s) \right|^2 ds \\ & + W^2 \int_{\mathrm{S}_1} \left| \boldsymbol{\nu} \times [\boldsymbol{H}^{\mathrm{d}}_{1N} + \boldsymbol{H}^{\mathrm{i}} - \boldsymbol{H}^{\mathrm{d}}_{2N}](s) \right|^2 ds \\ & + W^2 \int_{\mathrm{S}_2} \left| \boldsymbol{\nu} \times [\boldsymbol{H}^{\mathrm{d}}_{2N} - \boldsymbol{H}^{\mathrm{d}}_{3N}](s) \right|^2 ds \end{aligned} \tag{17}$$

where S_1 and S_2 denote one period of the upper and the lower surface, $\boldsymbol{\nu}$ is a unit normal vector to the surfaces, and W is an intrinsic impedance of vacuum.

We discretize the quadratic form I_N by the trapezoidal rule to have a discretized least-squares problem. We notice in (15) that there are $8(2N+1)$ unknown coefficients in total. It is known that the sufficient number of equations in the least-squares approximation is twice as many as the number of unknowns [8]. Hence, locating $J = 2(2N + 1)$ equally-spaced sampling points (with respect to x) on one period of both S_1 and S_2 and describing the boundary conditions at these points, we have $16(2N + 1)$ linear equations for the coefficients. We solve this over-determined set of equations in the least-squares sense employing a QR-decomposition algorithm [9].

3. NUMERICAL RESULTS AND EXPERIMENTAL DATA

In this section we show some numerical results for TM-wave incidence obtained by the method in Section 2, the results which confirm the possibility that the resonance absorption can be used in index measurement [5, 10]. The numerical results will be compared with experimental data.

3.1. Preparation for Numerical Computation and Experiment

We define the efficiency of the zeroth-order diffracted mode in V_1 as per period power carried away by the zeroth mode normalized by the per period incident power:

$$\rho_0 = \rho_0^{\mathrm{TE}} + \rho_0^{\mathrm{TM}} \tag{18}$$

where the efficiency of the zeroth-order TE and TM mode is given by

$$\rho_0^{\mathrm{TE}} = (\gamma_{10}/\gamma)\left|A_{10}^{\mathrm{TE}}\right|^2,\ \rho_0^{\mathrm{TM}} = (\gamma_{10}/\gamma)\left|A_{10}^{\mathrm{TM}}\right|^2 \tag{19}$$

A_{10}^{TE} and A_{10}^{TM} are the modal coefficients of the zeroth-order TE and TM mode. In the following examples we employ a commercial ultra violet (UV) grating made of aluminum (Al) with a thin gold (Au) over-coating, whose parameters are $2h = 0.061\,\mu$m, $d = 0.556\,\mu$m and $e = 0.044\,\mu$m. The incident light is a monochromatic TM plane wave from a laser diode (LD) with $0.660\,\mu$m wavelength. The refractive indices of Au and Al at this wavelength are $n_2 = 0.1355 + i3.4679$ and $n_3 = 1.3517 + i7.1150$ [11]. In an experiment we observe the TE- or TM-component of the zeroth-order diffracted power using a photodiode with a polariser.

Figure 3 shows the experimental setup. As shown in this figure, a commercial UV grating made of Al with a thin Au over-coating is mounted on a stage that rotates about the Z-axis to set the azimuth angle ϕ. The incident light is set on a rotating arm that allows polar angle θ scan with 0.2° steps. The TE- or TM-component of the zeroth-order diffracted wave is monitored by a photodiode (PD) through a polariser.

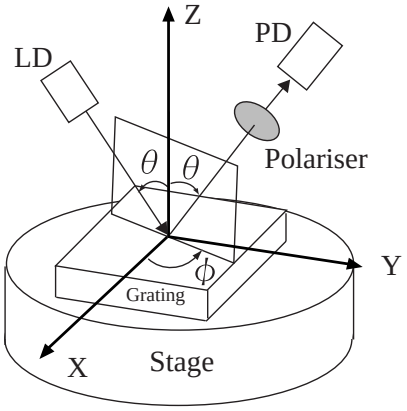

Figure 3. The experimental setup.

3.2. Numerical Results and Experimental Data

First we show typical plasmon resonance absorption in planar mounting in Fig. 4. The solid curve and the broken curve represent numerical result and experimental data. We observe good agreement

between them. The dip in the efficiency at $\theta = 8.2°$ corresponds to the absorption, while the sharp peak at $\theta = 10.6°$ relates the -1 order cutoff.

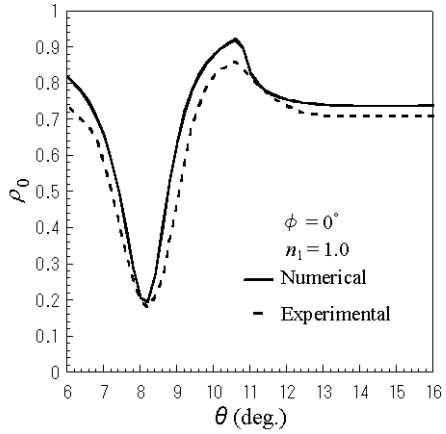

Figure 4. Typical absorption in planar mounting ($\phi = 0°$).

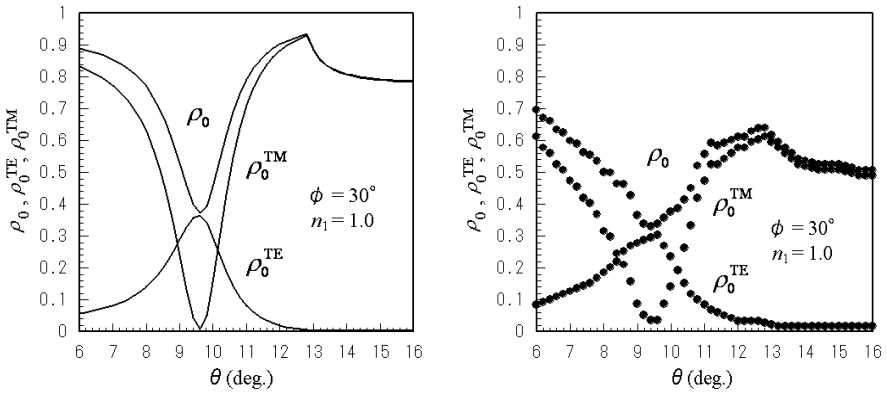

Figure 5. ρ_0, ρ_0^{TE} and ρ_0^{TM} as functions of θ ($\phi = 30°$), (a) numerical results, (b) experimental data.

The next illustration, Fig. 5, is an example of the absorption in conical mounting. We set $\phi = 30°$ and obtained the zeroth-order efficiency ρ_0 and its TM- and TE-component (ρ_0^{TM} and ρ_0^{TE}) as functions of θ. The solid curves in Fig. 5(a) show numerical results and the dots in Fig. 5(b) represent the experimental data. We observe

fairly good agreement between the numerical results and experimental data. The difference in the magnitude of efficiency is caused by the loss of the polariser. We observe partial absorption of incident light as the dip of ρ_0 at $\theta = 9.6°$ followed by a sharp peak at $\theta = 12.8°$. The dip is caused by excitation of plasmons and the peak is the result of the -1 order cutoff. It appears that the absorption is not so strong as that in the planar mounting case. We, however, notice the strong TM-TE mode conversion [4, 5] accompanying the absorption: when the polar angle θ is in close vicinity to the resonance angle, ρ_0^{TM} almost vanishes, and ρ_0^{TE} is dominant in ρ_0.

The enhanced TM-TE mode conversion can be used in precise measurement of the resonance angle. For this purpose we define the ratio $\rho_0^{\mathrm{TE}}/\rho_0^{\mathrm{TM}}$ and illustrate it as a function of θ in Fig. 6. ϕ is a parameter and is shown in the figure. The solid curves in Fig. 6(a) show numerical results and the broken curves in Fig. 6(b) represent the experimental data. Although the absorption dips are not sufficiently sharp, the ratio shows a sharp peak for a specific ϕ: in this example this can be seen at $\phi = 30°$ in both numerical and experimental result. Thus, we can find the resonance angle with four digits accuracy in a preliminary experiment without much trouble.

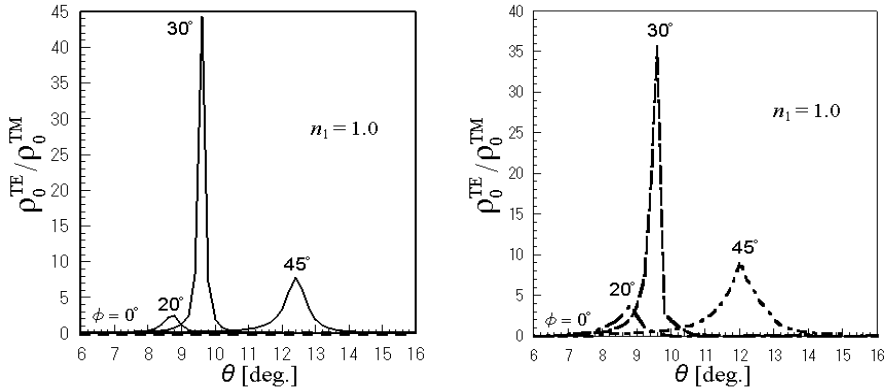

Figure 6. $\rho_0^{\mathrm{TE}}/\rho_0^{\mathrm{TM}}$ as functions of θ, (a) numerical results, (b) experimental data.

Because the absorption is caused by the excitation of a surface wave, the resonance angle is a sensitive function of the refractive index of a material in V_1, which has been assumed to be vacuum in the above discussion. This suggests that TM-TE mode conversion accompanying the resonance absorption can be used for an index sensor. We expect

that the ratio $\rho_0^{\mathrm{TE}}/\rho_0^{\mathrm{TM}}$ can be employed in measuring the refractive index of the material in V_1. To examine this possibility we vary n_1 in a range from $n_1 = 1.348$ through 1.449 and show the numerical results in Fig. 7(a). Here, the material in V_1 is assumed to be solution of glycerin (glycerin + aq) whose index is given by $n_1 = 1.348$ (10% glycerin), 1.356 (20%), 1.384 (40%), 1.400 (50%), and 1.449 (100%). Fig. 7(b) represents the experimental data in which we observe good agreement between numerical results and experimental data. We also observe the change in concentration of samples from 10% through 100% is therefore detected as a shift of a resonance angle θ from 18.2° to 27.0°. We have confirmed numerically that: we can realize a 750 degrees/RIU (Refractive Index Unit) resolution by adopting the appropriate azimuth angle ϕ and polar angle θ, the resolution which is ten times more sensitive than a conventional prism-based plasmon index sensor. [5]

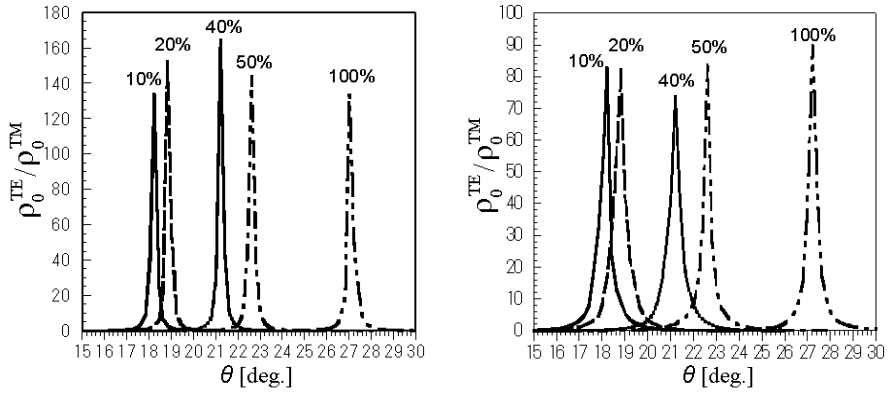

Figure 7. Comparison of the ratio $\rho_0^{\mathrm{TE}}/\rho_0^{\mathrm{TM}}$ obtained by experiment with the numerical results ($\phi = 30°$), (a) numerical results, (b) experimental data.

4. CONCLUSION

Enhanced TM-TE mode conversion caused by excitation of plasmons on a metal grating placed in conical mounting has been examined numerically and the results have compared with experimental data. The azimuth angle ϕ has large influence on the location and strength of the TM-TE mode conversion. For TM-wave incidence the TM-component of the diffracted wave almost vanished and the TE-component was dominant in close vicinity to the resonance angle.

The ratio of diffraction efficiency $\rho_0^{\mathrm{TE}}/\rho_0^{\mathrm{TM}}$ having a sharp peak at the resonance angle, hence, could be a good measure in finding the refractive index because the resonance angle is sensitive to the index. Results of a preliminary experiment confirmed that we could find the angle to a 0.1° accuracy. If we apply the resonance absorption to an index sensor, the accuracy means four digits determination of the refractive index of a material over the grating surface. If necessary precision in the experiment could be insured, determination of the refractive index to more than four digits would be achieved without much trouble.

ACKNOWLEDGMENT

This work was supported in part by Grants-in-Aid for Scientific Research from Japan Society for the Promotion of Science (Grant number 17560313).

REFERENCES

1. Raeter, H., "Surface plasmon and roughness," *Surface Polaritons*, V. M. Argranovich and D. L. Mills (eds.), 331–403, North-Holland, New York, 1982.
2. Nevièr, M., "The homogenous problem," *Electromagnetic Theory of Gratings*, R. Petit (ed.), 123–157, Springer-Verlag, Berlin, 1980.
3. Barnes, W. L., T. W. Preist, S. C. Kitson, J. R. Sambles, N. P. K. Cotter, and D. J. Nash, "Photonic gaps in the dispersion of surface plasmons on gratings," *Phys. Rev. B*, Vol. 51, 11164–11167, 1995.
4. Bryan-Brown, G. P., J. R. Sambles, and M. C. Hutley, "Polarization conversion through the excitation of surface plasmons on a metallic grating," *J. Modern Optics*, Vol. 37, No. 7, 1227–1232, 1990.
5. Matsuda, T., D. Zhou, and Y. Okuno, "Numerical analysis of TE-TM mode conversion in a metal grating placed in conical mounting," *IEICE Trans. Electron.*, Vol. J82-C-I, No. 2, 42–49, 1999 (in Japanese).
6. Yasuura, K. and T. Itakura, "Approximation method for wave functions (I), (II), and (III)," Kyushu Univ. Tech. Rep., Vol. 38, No. 1, 72–77, 1965; Vol. 38, No. 4, 378–385, 1966; Vol. 39, No. 1, 51–56, 1966 (in Japanese).

7. Yasuura, K., "A view of numerical methods in diffraction problems," *Progress in Radio Science*, W. V. Tilson and M. Sauzade (eds.), 1966–1969, 257–270, URSI, Brussels, 1971.
8. Okuno, Y. and H. Ikuno, "Yasuura's method, its relation to the fictitious source methods, and its advancements in solving 2-D problems," *Generalized Multipole Techniques for Electromagnetic and Light Scattering*, Th. Wriedt (ed.), 111–141 Elsevier, Amsterdam, 1999.
9. Lawson, C. L. and R. J. Hanson, *Solving Least-Squares Problems*, Prentice-Hall, Englewood Cliffs, NJ, 1974.
10. Matsuda, T. and Y. Okuno, "Resonance absorptions in a metal grating with a dielectric overcoating," *IEICE Trans. Electron.*, Vol. E76-C, No. 10, 1505–1509, 1993.
11. Hass, G. and L. Hadley, "Optical properties of metals," *American Institute of Physics Handbook*, 2nd edition, D. E. Gray (ed.), 6–107, McGraw-Hill, New York, 1963.